Journal of Inorganic Biochemistry 251 (2024) 112452

Contents lists available at ScienceDirect

Journal of Inorganic Biochemistry

journal homepage: www.elsevier.com/locate/jinorgbio

Cytotoxic auranofin analogues bearing phosphine, arsine and stibine ligands: A study on the possible role of the ligand on the biological activity

Ester Giorgi [a], Michele Mannelli [b], Tania Gamberi [b], Maria Durante [a], Chiara Gabbiani [a], Damiano Cirri [a,*], Alessandro Pratesi [a,*]

[a] Department of Chemistry and Industrial Chemistry, University of Pisa, Via G. Moruzzi 13, 56124 Pisa, Italy
[b] Department of Experimental and Clinical Biomedical Sciences "Mario Serio", University of Florence, Viale G.B. Morgagni 50, 50134 Firenze, Italy

ARTICLE INFO

Keywords:
Auranofin
Anticancer drugs
Arsenic
Antimony
Gold
Metal-based complexes

ABSTRACT

Three gold(I) linear compounds, sharing the general formula [AuI(LPh_3)], have been synthesized and characterized. The nature of the ligand has been modified by moving down among some of the elements of group 15, i.e. phosphorus, arsenic and antimony. The structures of derived compounds have been solved through XRD and the reactivity behaviour towards selected biomolecules has been investigated through a multi-technique approach involving NMR, high-resolution mass spectrometry and IR. Moreover, the biological activity of the investigated compounds has been comparatively analyzed through classical methodologies and the disclosed differences are discussed in detail.

1. Introduction

In the context of chemotherapeutic drugs, platinum-based complexes have dominated the scene for decades, remaining among the most effective and employed treatments [1,2]. However, they present significant limitations, such as severe side effects, frequent occurrence of intrinsic or acquired resistance and the possibility of cancer relapse, especially for certain types of cancer [3,4]. In this frame, the scientific community has been spurred towards an intensive search for new anticancer metallodrugs based on different metal center, among which ruthenium, palladium and gold play an important role [1,5–10]. Since the disclosing of cytotoxic properties of the antirheumatic drug auranofin (AF, Fig. 1), this compound and more in general the Au(I)-based compounds, have been extensively studied with the aim of finding better anticancer drugs with respect to the well-known platinum-based compounds [11,12]. Anyway, despite the promising preliminary results, auranofin has still not gained FDA approval for any neoplastic diseases; however, this spurred the interest of the bioinorganic chemists' community to work on more effective and selective gold-based compounds [13,14]. Among all the newly synthesized compounds, the phosphine-gold(I) linear compounds represent a promising class endowed of an even better pharmacological profile with respect to auranofin itself, such as higher cytotoxicity and selectivity towards cancer cells [15–18].

This approach involves the systematic modification of different portions of the auranofin structure, including the substitution of the phosphine moiety with other ligands [19], the functionalization with biologically relevant molecules [20], and the fine-tuning of the metal centre reactivity through the replacement of the thioglucosetetraacetate with different halides or pseudohalides [21,22]. These modifications can potentially result in new gold(I) complexes with enhanced cytotoxicity, improved pharmacokinetic properties, and reduced toxicity towards healthy cells [16]. The abundant literature on auranofin provides various information about the effects of small structural changes on its activity [15]. In 2017 some of us reported the synthesis of [AuI(PEt_3)], an analogue of AF bearing an iodine atom in the place of thioglucose moiety [17,21]. In comparison with AF and [AuCl(PEt_3)], [AuI(PEt_3)] shows higher lipophilic properties and, interestingly, still a similar cytotoxic effect towards four CRC cell lines, with IC_{50} values falling in the nanomolar range and no cytotoxic activity on healthy cells (human fibroblast cell line and human embryonic kidney cells). These results highlight that the presence of the thiosugar moiety is not strictly correlated with the cytotoxic potential, being this latter almost exclusively attributable to the $[Au(PEt_3)]^+$ cation. Moreover, other works well show how tuning some relevant chemical properties, such as lipophilicity and water solubility, can be useful to improve bioavailability, and then the overall pharmacological activity. Indeed, the *in vivo* profile obtained for [AuI(PEt_3)] on the murine model presents a considerable improvement with respect to AF [16]. Another example where the

* Corresponding authors.
E-mail addresses: damiano.cirri@unipi.it (D. Cirri), alessandro.pratesi@unipi.it (A. Pratesi).

https://doi.org/10.1016/j.jinorgbio.2023.112452
Received 25 September 2023; Received in revised form 24 November 2023; Accepted 1 December 2023
Available online 3 December 2023

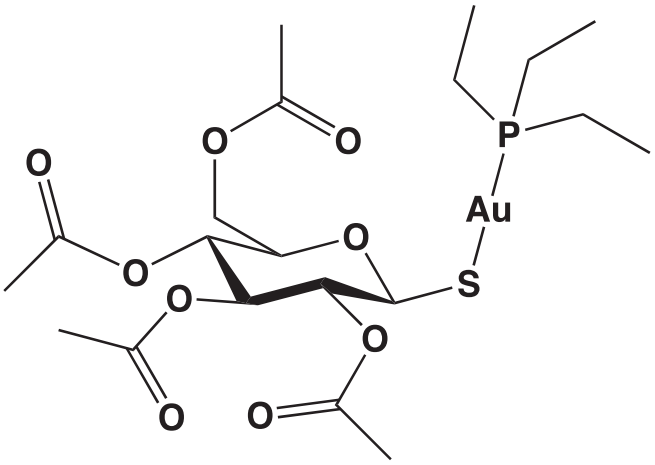

Fig. 1. Auranofin (1-Thio-β-*D*-glucopyranosatotriethylphosphine gold-2,3,4,6-tetraacetate) structure. (For interpretation of the references to colour in this figure legend, the reader is referred to the web version of this article.)

thioglucosetetraacetate ligand has been replaced, obtaining interesting differences in the activity, is AFETT ((ethylthiosalicylate(triethylphosphine)gold(I)) [20]. This latter compound has been designed taking inspiration from AF as well as the Hg-based complex thimerosal, replacing AF's thioglucosetetraacetate with an ethylthiosalicylate moiety. Compared to auranofin, AFETT features some peculiar and unique characteristics such as lower lipophilicity, higher water solubility and a prompter reactivity towards the investigated target biomolecules. Because of these differences, AFETT could exhibit considerable pharmaceutical and therapeutic advantages over auranofin itself [20]. Another strategy investigated by our group for designing new AF analogues involves the modification of phosphine ligand, which is part of the pharmacologically active $[Au(PEt_3)]^+$ fragment, as opposed to the thioglucosetetraacetate which mainly has a "functional" role [23]. For example, our research group recently reported the synthesis of a panel of AF's analogues in which triethylphosphine was replaced with a trimethylphosphite ligand, while the gold(I) linear coordination was completed with halide or thioglucose tetraacetate moiety [19]. All the newly synthesized compounds showed stability in aqueous solution, but significant differences with respect to auranofin were highlighted when interacting with some selected target proteins [19].

In the frame of the discussed modification strategies, we synthesized three new complexes where the triethylphosphine ligand of the promising $[AuI(PEt_3)]$ complex was replaced by triphenylphosphine, triphenylarsine and triphenylstibine (Fig. 2). The substitution of phosphorus with other atoms of the same group should lead to a different coordination bond strength and, hence, to a different reactivity of the entire molecule. Another appealing factor is the possible synergistic effect, which refers to the advantageous interaction of different therapeutic agents [24], obtained through the combined action of gold with As and Sb. More in detail, both arsenic and antimony present cytotoxic features

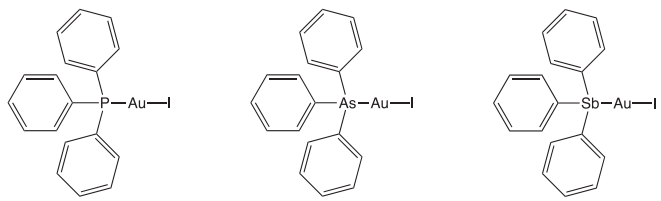

Fig. 2. Structures of the three new Au(I) complexes.

in the anticancer therapies context, although only arsenic is currently used in the clinic for the treatment of relapsed acute promyelocytic leukaemia (APL) as arsenic trioxide [25,26]. Nevertheless, antimony is employed as an antiparasitic agent in the treatment of leishmaniasis [27,28].

2. Results and discussion

2.1. Synthesis and characterisation

The first gold(I) complex in this series, i.e., $[AuI(PPh_3)]$ (**1**), was obtained through a simple ligand exchange reaction, in which the commercially available $[AuCl(PPh_3)]$ was reacted with 5 equivalents of KI. The reaction produced $[AuI(PPh_3)]$ in an almost quantitative yield (92%). For the synthesis of compounds **2** and **3**, $[AuCl(SMe_2)]$ was reacted with triphenylarsine and triphenylstibine, respectively, to obtain the chloride complexes where the Au centre is coordinated with As or Sb, affording the $[Au(AsPh_3)Cl]$ and $[AuCl(SbPh_3)]$ complexes. These latter products were reacted with KI to obtain the corresponding iodide complexes $[Au(AsPh_3)I]$ and $[AuI(SbPh_3)]$ (**2** and **3**, Fig. 2).

2.2. Crystal obtainment and XRD analysis

Crystals suitable for XRD analysis have been collected for $[Au(AsPh_3)I]$ and $[AuI(SbPh_3)]$ through slow evaporation of $CDCl_3$ from samples previously prepared for the NMR analysis, whilst the crystallographic structure for $[AuI(PPh_3)]$ was already published [29–31]. As expected, the analysis of both complexes shows the typical linear coordination geometry of the Au(I) metal center. Interestingly, both the crystallographic structure shows the peculiar direct interaction between the Au (I) centre of one molecule and the gold atom of another adjacent molecule, and this dimer is repeated throughout all the crystal (Fig. 3). The Au—Au bond length is 2.9896(2) Å for $[Au(AsPh_3)I]$ and 2.9903(5) Å for $[AuI(SbPh_3)]$. This peculiar Au—Au intermolecular bond has been already described by some of the authors for other gold(I)-phosphine complexes [20].

Crystal data and refinement parameters are reported in Tables S1-S16. CCDC contains the supplementary crystallographic data for this paper (deposition number: 2296797 for $[Au(AsPh_3)I]$ and 2296798 for $[AuI(SbPh_3)]$).

2.3. In solution behaviour

LogP determination plays a crucial role in understanding the properties of a potential drug. LogP helps assess the compound's lipophilicity, which impacts its solubility, permeability, uptake, and systemic distribution. This information aids in predicting the drug's absorption, bioavailability, and potential for crossing cellular membranes. From LogP evaluation studies the three $[AuI(LPh_3)]$ compounds were found to be particularly lipophilic. The LogP values have been reported in Table 1. The three new compounds are characterized by greater lipophilicity than both auranofin and $[AuI(PEt_3)]$, due to the presence of the three phenyl groups compared to the ethyl groups present in the latter two complexes. In addition, a slight decrease in lipophilicity is observed when moving from P to As to Sb, in accordance with the increase in the metallic character of the elements moving down the group.

Stability studies in solution with DMSO were carried out by monitoring the compounds through ^{31}P NMR and ^{13}C NMR. The latter showed that complex **1** remains stable in solution for at least 24 h, while complexes **2** and **3** present instability after 1 h, as evidenced by the shift of characteristic signals in ^{13}C NMR spectra (See Supporting Information).

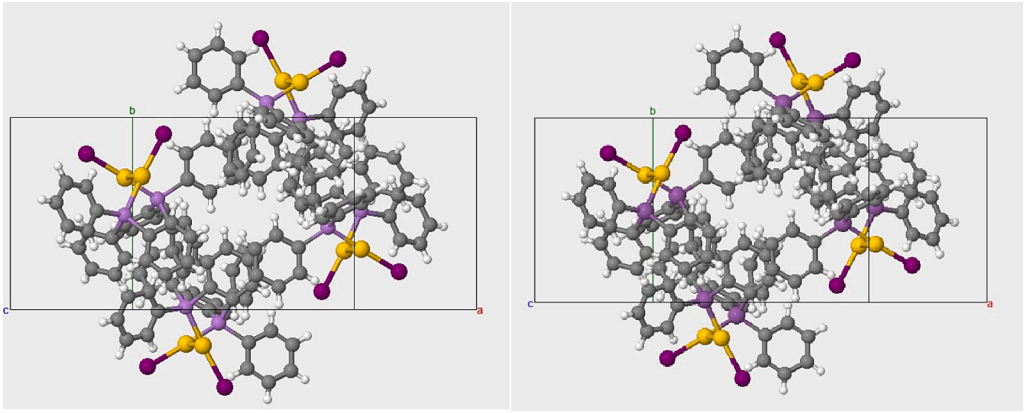

Fig. 3. Crystal structure of [Au($AsPh_3$)I] (left) and [AuI($SbPh_3$)] (right).

Table 1
Octanol–water partition coefficients at 25 °C ($logP_{O/W}$, ICP-OES).

Complex	$LogP_{O/W}$
Auranofin	1.6[a]
[AuI(PEt_3)]	4.6[a]
[AuI(PPh_3)], **1**	5.2
[Au($AsPh_3$)I], **2**	5.1
[AuI($SbPh_3$)], **3**	5.0

[a] $LogP_{O/W}$ value retrieved from the literature. [21,32].

2.4. Interaction with biologically relevant amino acids

Although the overall mechanism of action of anticancer gold-based complexes has not been completely clarified yet, one of the most involved targets seems to be thioredoxin reductase (TrxR) [33,34]. This enzyme is involved in maintaining cellular redox homeostasis in physiological conditions and is usually overexpressed in cancer cells. The inhibition of TrxR by gold(I) complexes can lead to dysfunction of critical cellular processes and to apoptosis of cancer cells [34,35]. There are several indications that TrxR inhibition could happen from the direct coordination of the gold(I) center to the functional selenocysteine present in the active site [36,37]. Moreover, some other important protein targets seem to be involved in the mechanism of action of gold-based complexes [38]. Indeed, has been reported that some gold compounds induce apoptosis in cancer cells by interacting with proteins involved in apoptosis pathways, such as Bcl-2 and Bax [39]; proteins involved in cell cycle regulation, such as cyclins and cyclin-dependent kinases (CDKs) [40]; the vascular endothelial growth factor (VEGF) and its receptors [40], and metallothioneins [41].

In order to understand the interaction mechanisms between these new gold(I) complexes and the main target TrxR, the use of molecular simplified models is worthwhile [42]. For instance, two short peptides have been previously synthesized in our group, that can be exploited in interaction studies as reduced models. These synthetic peptides, indeed, represent a critical portion of the enzyme's structure and allow controlled studies of the interaction with gold(I) complexes. Furthermore, interaction studies with amino acids present in the active site of TrxR are advantageous for elucidating the specific interaction between gold(I) complexes and the enzyme [43,44]. Cysteine and selenocysteine, being present in the active site of the enzyme, play a key role in the redox catalytic function of the TrxR [45]. The study of the interaction with such simplified models may give a preliminary indication of the complexes' potential reactivity with the target TrxR [46].

Thus, interaction studies with the amino acid cysteine and selenocysteine were carried out. Firstly, we explored the reactivity of the three new complexes with L-cysteine hydrochloride monohydrate (in 1:1.1 amino acid to metal complex ratio) through NMR experiments. They were carried out in DMSO, owing to solubility issues for the investigated complexes. As shown in NMR spectra, all the complexes readily react with Cys. More precisely, in the case of incubation with [AuI(PPh_3)] (Fig. 4), the peak of the Cys-S-[Au(PPh_3)] adduct (37.575 ppm) is immediately visible in the ^{31}P NMR spectrum and no further changes are observable after 24 h of incubation. As a proof of concept, the ^{31}P chemical shift value of the adduct is in agreement with those reported for similar R-S-[Au(PPh_3)] compounds [47]. On the other hand, the reactivity of [Au($AsPh_3$)I] and [AuI($SbPh_3$)] towards Cys, monitored through ^{13}C NMR, tuned out to be completely different. Indeed, for both compounds is clearly visible only the formation at t_0 of cystine (Figs. 5 and 6). Notably, the ESI-MS experiments confirmed this hypothesis (see later sections). Anyway, after 24 h of incubation, ^{13}C NMR spectra suggest the oxidative formation of cystine. This latter aspect was also confirmed by the comparison of pink/violet coloration attributable to the formation of dispersed elemental gold [48]. The formation of cystine was further confirmed by comparing the ^{13}C chemical shifts with those belonging to the cystine spectrum shown in Fig. S16 (Supporting Information). This latter was obtained by stirring L-cysteine hydrochloride monohydrate in water for a week.

The reactivity of Cys with the three complexes [AuI(LPh_3)] (**1**–**3**) was also investigated through IR spectroscopy. In particular, Cys was stirred for 2 h in the presence of each [AuI(LPh_3)] complex in DMSO; then, after the removal of the solvent, the solid residue was suspended in liquid paraffin and analyzed in nujol. The collected spectra were compared with the IR profile of Cys in the same solvent. In every case, the infrared spectra showed the disappearance of the absorption band at 2564 cm^{-1}, assigned to the cysteine S—H stretching mode [49]. Figs. 7, 8 and 9 display the superimpositions between the IR spectra of the unreacted Cys and of the reaction crude, where it is possible to notice the disappearance of the diagnostic band. The IR data agree with ^{31}P NMR and ^{13}C NMR experiments, suggesting the suppression of S—H stretching mode due to the formation of a gold/Cys adduct (for the reaction with [AuI(PPh_3)]) or through oxidative dimerization of cysteine to cystine (for the reaction with [AuI($AsPh_3$)] and [AuI($SbPh_3$)]).

In order to confirm the reactivity of these compounds with cysteine, high-resolution ESI-MS experiments were also conducted. The data obtained from this additional independent investigation were in excellent agreement with those derived from NMR and IR. Specifically, in the case of [AuI(PPh_3)], the peak at *m/z* 580 has been attributed to the formation of the Cys-[Au(PPh_3)] adduct (Fig. S17). However, in the case of compounds [Au($AsPh_3$)I] and [AuI($SbPh_3$)], no formation of adducts with the amino acid was observed even with this technique. For both, the formation of cystine is evident, as indicated by the presence of the peak at *m/z* 241 (Fig. S18 and S19, respectively). Unfortunately, from the obtained data it is not possible to gain useful information regarding the

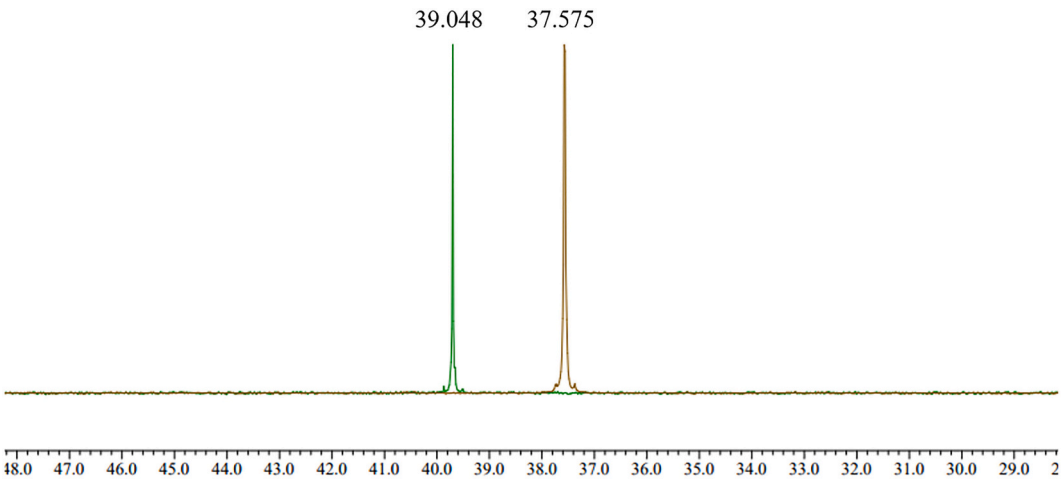

Fig. 4. ^{31}P NMR spectra in DMSO-d_6 of complex [AuI(PPh_3)] (green), [AuI(PPh_3)]/cysteine just after mixing (brown). (For interpretation of the references to colour in this figure legend, the reader is referred to the web version of this article.)

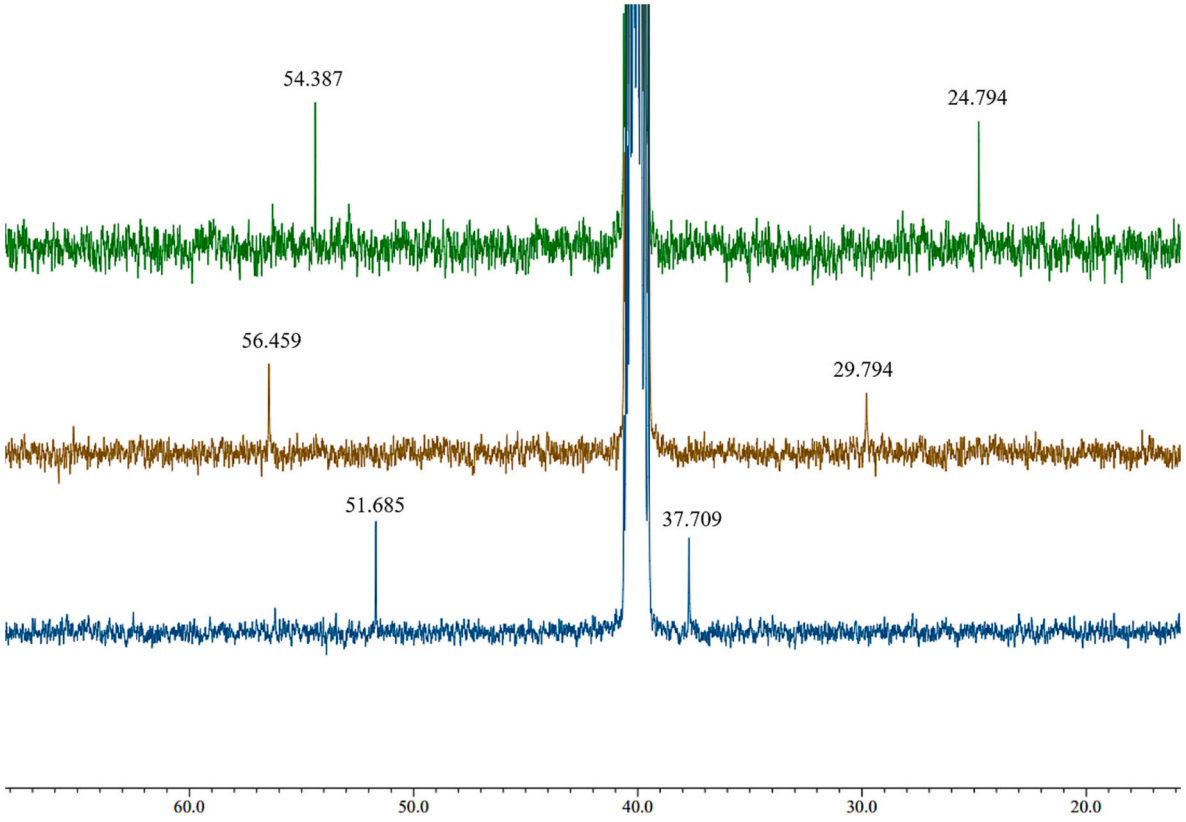

Fig. 5. ^{13}C NMR spectra in DMSO-d_6 of cysteine (green), [Au($AsPh_3$)I]/cysteine just after mixing (brown), [Au($AsPh_3$)I]/cysteine after 24 h of incubation at 37 °C (blue). (For interpretation of the references to colour in this figure legend, the reader is referred to the web version of this article.)

fate of ligands containing As and Sb.

ESI-MS was used also to conduct interaction studies with selenocysteine, since the previously used techniques, such as NMR and IR, in this case were not applicable. To this aim, the [AuI(LPh_3)] complexes were incubated in the presence of selenocysteine, in DMSO. Since this amino acid is commercially available as selenocystine, the sample preparation requires a preliminary step, a reduction reaction with DTT, to give the reactive selenol group. After 24 h of incubation at 37 °C with [AuI(PPh_3)], a cluster peak with the most intense signal at *m/z* 532 assignable to the Sec-Au-Sec adduct appeared (SI, Fig. S20). This signal cluster show the characteristic isotopic pattern of selenium. The superimposition of the experimental isotopic pattern with the theoretical one calculated for the hypothesized adduct confirmed the peak assignment. (SI, Fig. S21) The same situation occurs for complex [AuI($SbPh_3$)] (**3**) (SI, Fig. S22, S23), with the peak at *m/z* 532 representing, also in this case, the Sec-Au-Sec adduct. Conversely, it was not highlighted the formation of any adduct after the incubation with the complex [Au($AsPh_3$)I] (**2**) (see Supporting information).

2.5. ESI-MS interaction experiments with HSA

ESI mass spectrometry has become a valuable tool in recent years for

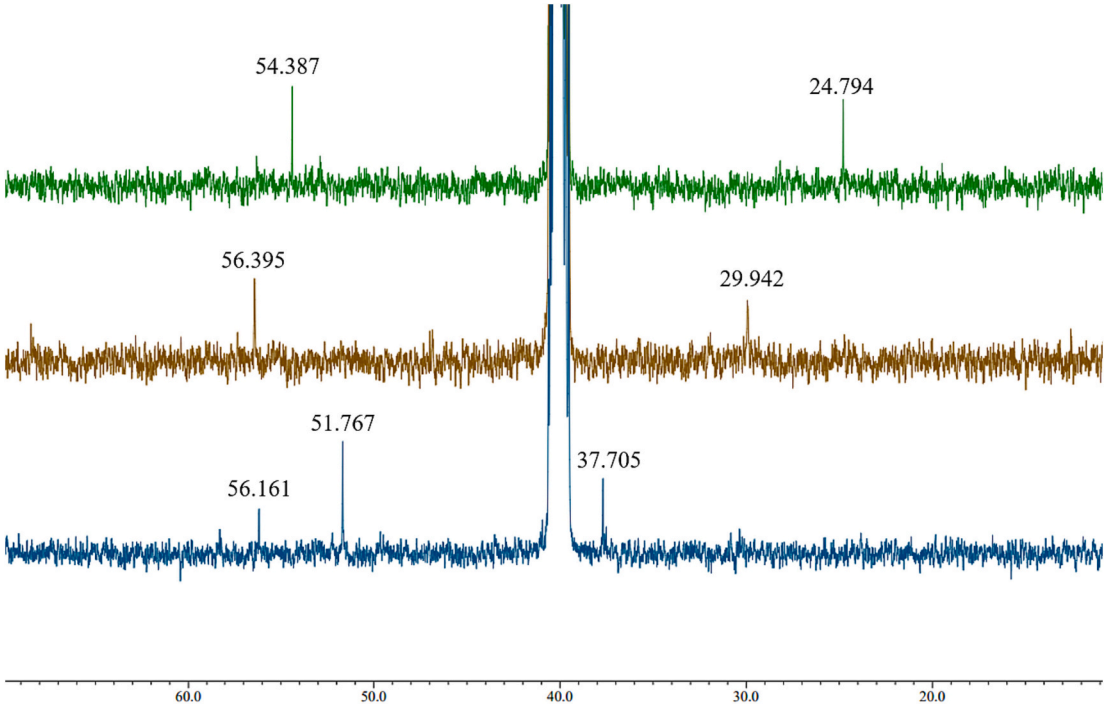

Fig. 6. ^{13}C NMR spectra in DMSO-d_6 of cysteine (green), [AuI($SbPh_3$)]/cysteine just after mixing (brown), [AuI($SbPh_3$)]/cysteine after 24 h of incubation at 37 °C (blue). (For interpretation of the references to colour in this figure legend, the reader is referred to the web version of this article.)

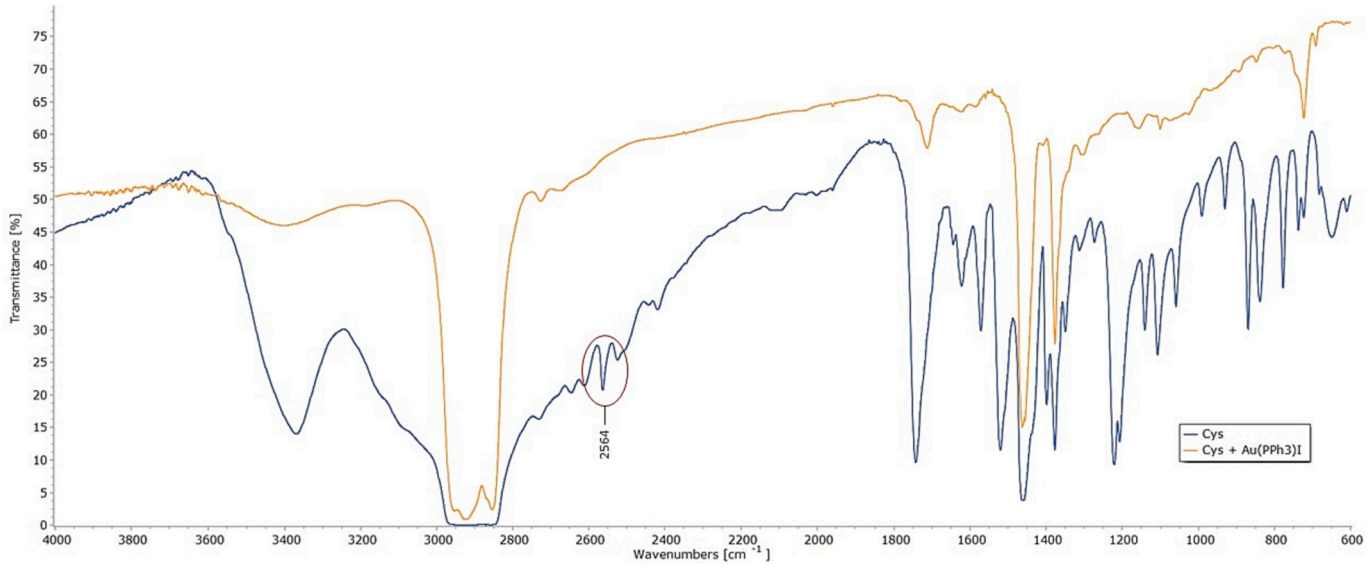

Fig. 7. IR spectra of Cys (blue line) and Cys reacted with [AuI(PPh_3)] (yellow line). (For interpretation of the references to colour in this figure legend, the reader is referred to the web version of this article.)

characterizing adducts formed between metal-based complexes and biomolecules, especially proteins of various sizes [38,50]. Using ESI-MS measurements, we investigated the reactions of the three [AuI(LPh_3)] complexes with a set of model proteins. The proteins selected for this analysis were human serum albumin (HSA), human carbonic anhydrase (hCA I), and bovine superoxide dismutase (SOD).

All three of the chosen proteins possess a free cysteine residue that can potentially undergo modification through coordination with the gold centre [51]. The proteins were individually incubated with the three [AuI(LPh_3)] complexes (**1–3**) at a fixed 2:1 metal-protein ratio for four hours at 37 °C. Then, ESI mass spectra were recorded for each sample under standard conditions and direct infusion.

The results revealed the formation of adducts between HSA and all three complexes. Notably, in the case of [AuI(PPh_3)], an adduct was observed where the gold centre retained coordination with the phosphine ligand (Fig. 10). Meanwhile, the reaction with [Au($AsPh_3$)I] and [AuI($SbPh_3$)] caused the loss of the ligands, indicating a weaker bond between the gold centre and As/Sb (Figs. 11 and 12). Notably, these latter data are in perfect agreement with the ^{13}C NMR experiments reported in Figs. 5 and 6. UV-Vis experiments were conducted to obtain more information on the evolution of the interaction between the three complexes and the HSA. The absorbance of albumin, in the presence of two equivalents of metal complexes, was followed for 24 h. However, no significant changes during the experiment were noticed (see Supporting

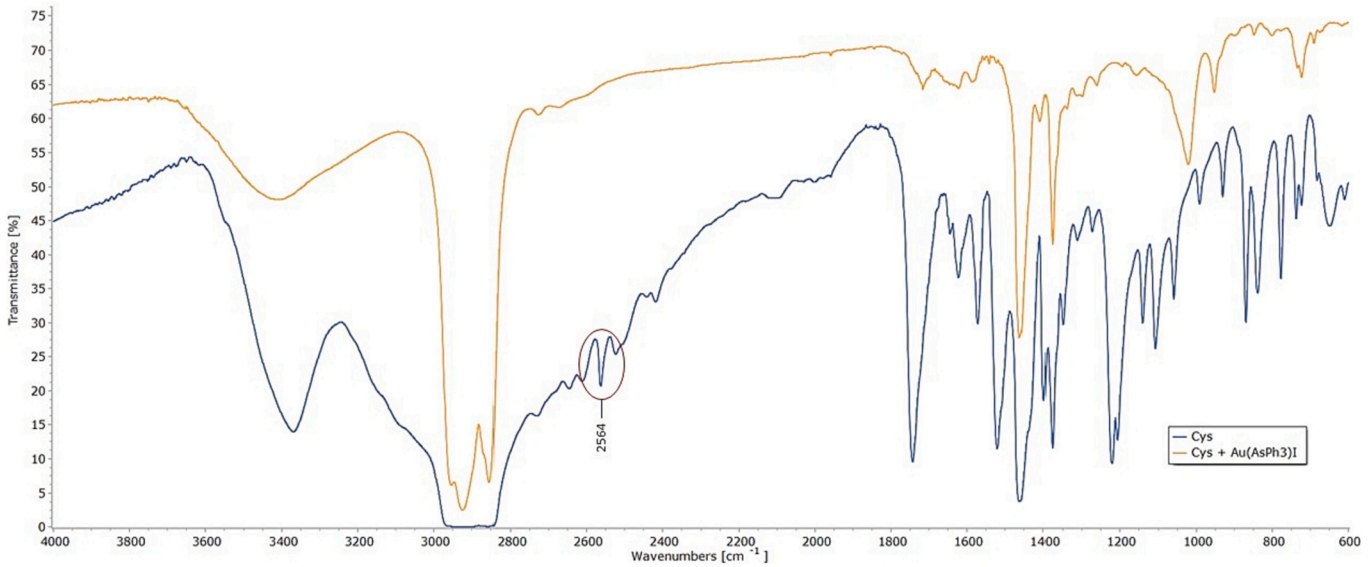

Fig. 8. IR spectra of Cys (blue line) and Cys reacted with [Au($AsPh_3$)I] (yellow line). (For interpretation of the references to colour in this figure legend, the reader is referred to the web version of this article.)

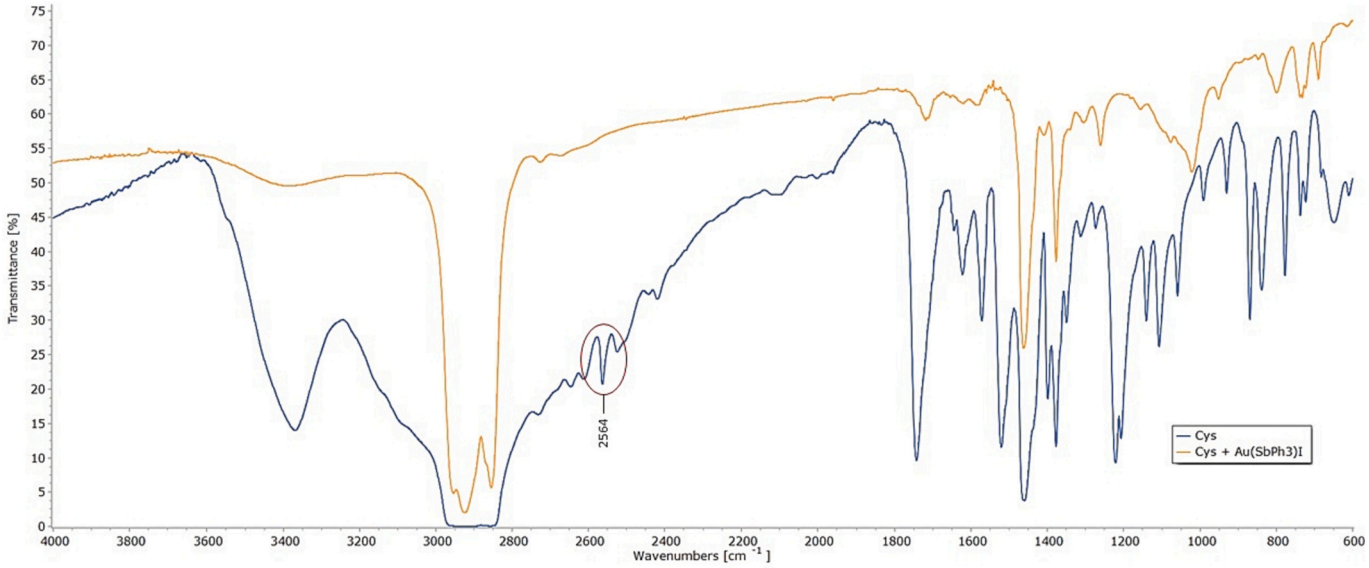

Fig. 9. IR spectra of Cys (blue line) and Cys reacted with [AuI($SbPh_3$)] (yellow line). (For interpretation of the references to colour in this figure legend, the reader is referred to the web version of this article.)

Information, Fig. S27-S29).

From experiments with hCA I, only in the case of [Au($AsPh_3$)I] the formation of an adduct could be detected (Fig. 13). In contrast, no adducts were detected with SOD, suggesting that the coordination is probably hindered due to the limited solvent accessibility of the free Cys residue (SI, Fig. S26). This result is consistent with previous studies conducted with auranofin [38].

2.6. Biological experiments

The antiproliferative properties of the three complexes [AuI(LPh_3)] (**1**–**3**) were evaluated by MTT (3-(4,5-Dimethylthiazol-2-yl)-2,5-diphenyltetrazolium bromide) test on cellular models of human ovarian cancer, i.e. A2780 cell line sensitive (A2780/S) and resistant (A2780/R) to cisplatin. As reported in Table 2, on A2780/S all complexes displayed potent growth inhibition effects with IC_{50} values in the low micromolar range, even though complex **1** was seven-fold more active with respect to complexes **2** and **3**. The antiproliferative effect decreased for both the three complexes towards the A2780/R cell line although their IC_{50} remain in the micromolar range and with values lower than that of cisplatin. The antiproliferative activity was also assessed on another human ovarian cancer cell line (i.e. SKOV-3) confirming the growth inhibition properties of both compounds and the higher potency of complex **1**. Remarkably, measuring their antiproliferative effects on the non-malignant cell line, human skeletal myoblasts (HSkM), the IC_{50} values were found to be higher (about 10-fold for complex **1**, 2-fold for **2** and **3**) suggesting a selectivity towards ovarian cancer cells (Table 2). Finally, by comparing the IC_{50} values of the three complexes on all the selected ovarian cancer cells with that of auranofin, we found that the cytotoxic potency of AF was higher. Interestingly, its cytotoxicity remains higher also in normal HSkM cell line. The same comparison has been made also with cisplatin and compounds **1**–**3** turned out far more

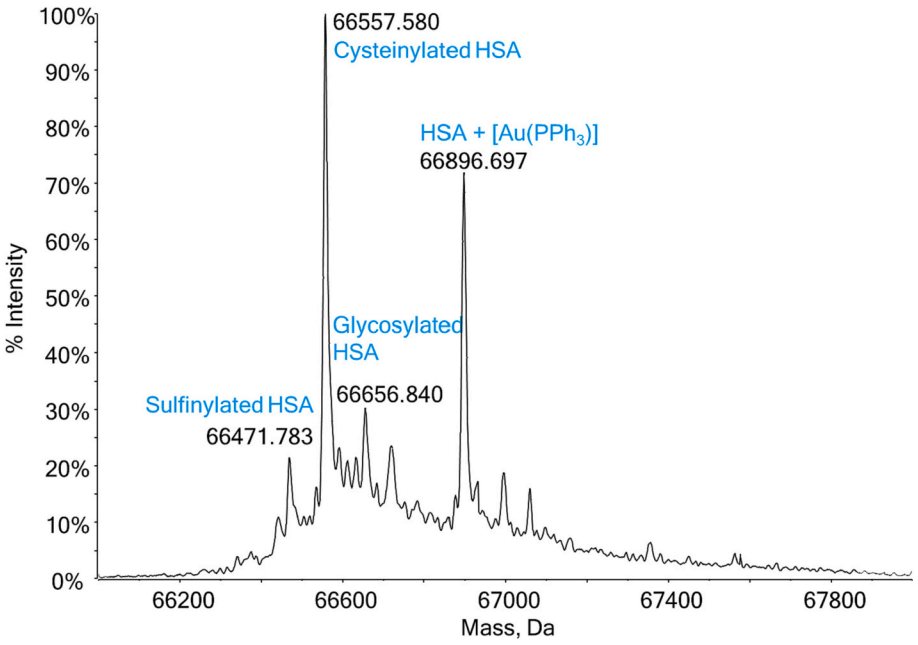

Fig. 10. Deconvoluted ESI-Q-TOF mass spectrum of HSA solution 10^{-6} M incubated for 4 h at 37 °C with [AuI(PPh_3)] (2:1 metal to protein ratio) in 20 mM ammonium acetate solution, pH 6.8. 0.1% of formic acid was added just before injection.

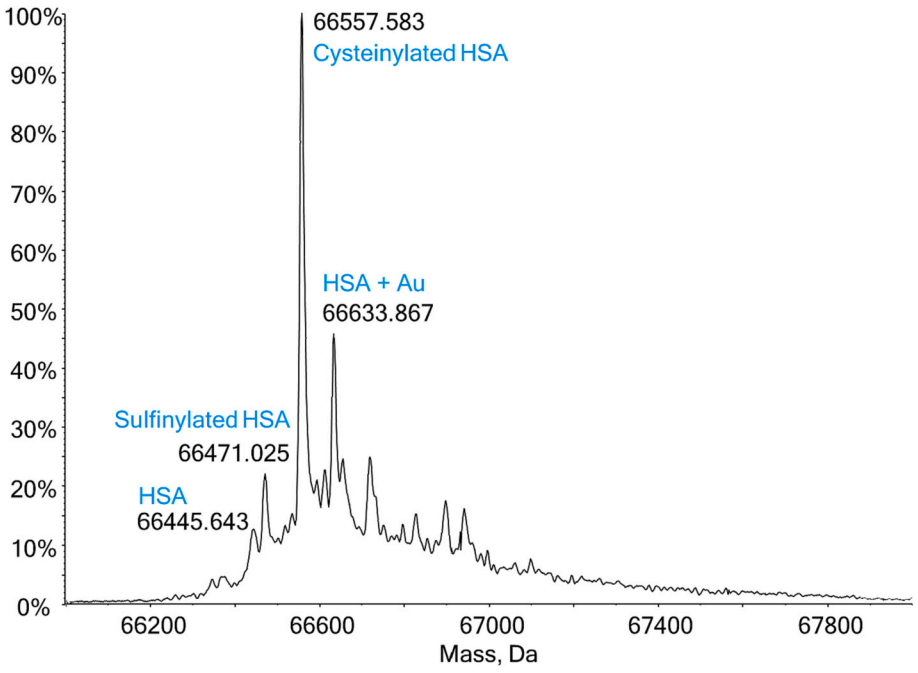

Fig. 11. Deconvoluted ESI-Q-TOF mass spectrum of HSA solution 10^{-6} M incubated for 4 h at 37 °C with [Au($AsPh_3$)I] (2:1 metal to protein ratio) in 20 mM ammonium acetate solution, pH 6.8. 0.1% of formic acid was added just before injection.

selective towards cancer cells with respect to the Pt-based metallodrugs. Moreover, in this comparison complex **1** also showed a better cytotoxic profile against all the selected cancer cell lines.

The thioredoxin reductase (TrxR) enzyme is established as the main target of gold-based compounds such as auranofin [54,55]. To prove whether the TrxR is also a likely target for the three complexes [AuI(LPh3)] (**1**–**3**), we selected A2780/S as model cancer cells and treated them for 24 h with a gold complex concentration corresponding to their 72 h-exposure IC_{50} dose. The results pointed out that the TrxR activity was not affected by complex **3** exposure, whereas it was significantly decreased with both complexes **1** and **2**. As reported in Fig. 14, complex **1** showed a greater inhibitory potency being able to reduce the enzyme activity by approximately 85% with respect to controls, followed in decreasing order of inhibition by auranofin (62%) and complex **2** (25%).

3. Experimental methods

3.1. Synthesis

3.1.1. [AuI(PPh_3)] (1)

85 mg of commercially available [AuCl(PPh_3)] have been suspended with 10 mL of methanol/acetone 1:1 solution in a 50 mL flask.

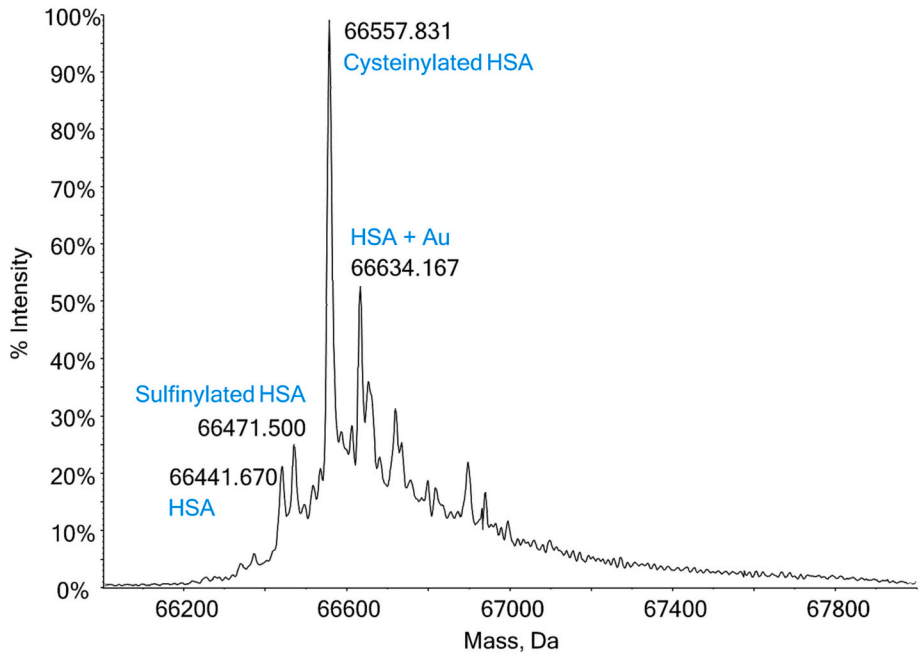

Fig. 12. Deconvoluted ESI-Q-TOF mass spectrum of HSA solution 10^{-6} M incubated for 4 h at 37 °C with [AuI($SbPh_3$)] (2:1 metal to protein ratio) in 20 mM ammonium acetate solution, pH 6.8. 0.1% of formic acid was added just before injection.

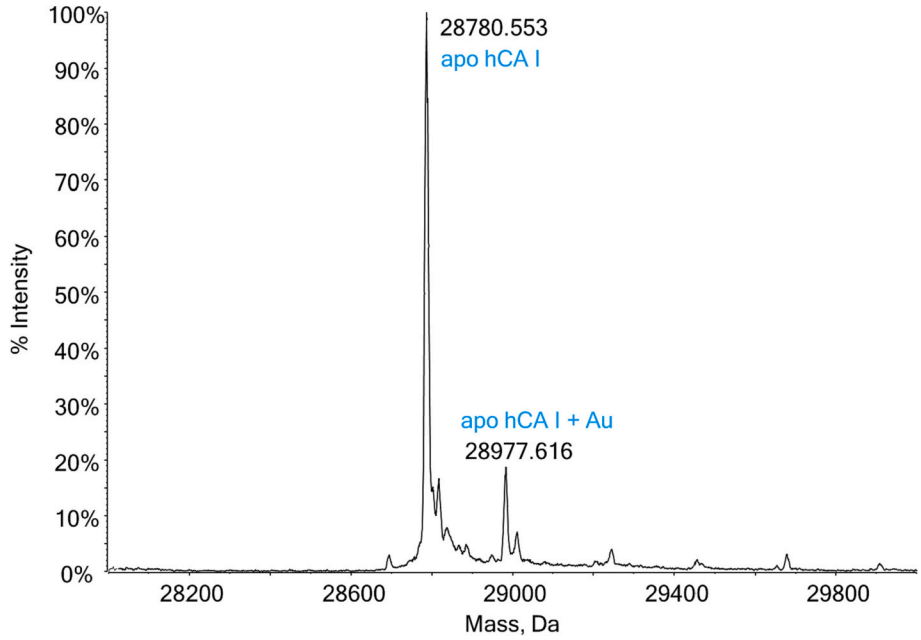

Fig. 13. Deconvoluted ESI-Q-TOF mass spectrum of hCA I solution 5×10^{-7} M incubated for 4 h at 37 °C with [Au($AsPh_3$)I] (2:1 metal to protein ratio) in 20 mM ammonium acetate solution, pH 6.8.

Subsequently, 120 mg (5.00 eq.) of KI were added and the resulting mixture was stirred at room temperature for 5 h. At the end of reaction time, the solvent was removed from the reaction flask through a rotary evaporator and the crude product was solubilized with dichloromethane. The solution was washed in a separation funnel with water and brine, then the organic phase was dried with anhydrous sodium sulphate. The resulting suspension was filtered to remove the wet sodium sulphate, then the solvent was removed under reduced pressure. The product was collected without needing further purifications as 92 mg of crystalline white solid (yield 92%).

^{1}H NMR (400 MHz, $CDCl_3$): 7.56–7.44 (m, 15H) ppm.

^{13}C NMR (100 MHz, $CDCl_3$): 134.19 (d, C_3, $J_{CP} = 14.3$ Hz), 131.96 (d, C_4, $J_{CP} = 2.9$ Hz), 129.35 (d, C_2, $J_{CP} = 11.5$ Hz), 129.24 (d, C_1, $J_{CP} = 58.5$ Hz) ppm.

^{31}P NMR (160 MHz, $CDCl_3$): 39.70 ppm.

Elemental analysis: [calc. %] C: 36.88; H: 2.58 [found %] C: 36.67H: 2.38.

3.1.2. *[Au($AsPh_3$)I] (2)*

175 mg of commercially available [AuCl(SMe_2)] have been solubilized with 10 mL of dichloromethane in a 50 mL flask. Subsequently, 182 mg (1.00 eq.) of triphenylarsine were added and the resulting

Table 2
Half-maximal inhibitory concentration (IC_{50}) after 72 h of treatment using MTT assay.

Complex	Cell line IC_{50} (μM) ± SD[a]				Selectivity index
	A2780/S	A2780/R	SKOV-3	HSkMC	HSkMC / A2780/S
[AuI(PPh_3)], (**1**)	1.9 ± 0.8	8.5 ± 0.9	3.5 ± 0.6	20.0 ± 1.2	10
[Au($AsPh_3$)I], (**2**)	13.13 ± 0.10	21.03 ± 0.14	14.5 ± 1.3	37.8 ± 1.3	3
[AuI($SbPh_3$)], (**3**)	14 ± 2	17.0 ± 0.6	10.62 ± 0.08	32 ± 3	2
Auranofin	0.73 ± 0.15	0.80 ± 0.05	1.3 ± 0.5	10.4 ± 1.1	14
Cisplatin	2.1 ± 0.2[b]	24.40 ± 0.10[c]	3.6 ± 0.8	6.3 ± 0.8	3

[a] Values are mean ± standard deviation (SD) of three biological independent experiments.
[b] Value retrieved from reference [52].
[c] Value retrieved from reference [53].

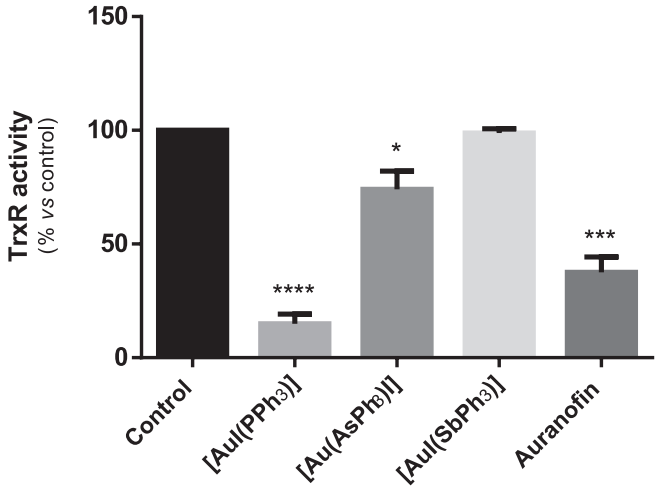

Fig. 14. Thioredoxin reductase (TrxR) activity in A2780/S cell line, treated for 24 h with gold complex concentrations corresponding to their 72 h-exposure IC_{50} doses. Values are mean ± standard deviation (SD) of three biological independent experiments. The statistical analysis was carried out using one-way ANOVA test followed by Tukey's multiple comparisons test using GraphPad Prism software v 6.0 (*$p < 0.05$; *** $p < 0.001$, **** $p < 0.0001$). (For interpretation of the references to colour in this figure legend, the reader is referred to the web version of this article.)

solution was stirred at room temperature. After 5 min, the dichloromethane was removed under reduced pressure and the solid residue was suspended in 10 mL of acetone. At this point, 240 mg (2.50 eq.) of KI were added to the suspension and the resulting mixture was stirred for 1 h. At the end of reaction time, the solvent was removed through a rotary evaporator and the crude product was solubilized in dichloromethane. The solution was washed in a separation funnel with water and brine, then the organic phase was dried with anhydrous sodium sulphate. The resulting suspension was filtered to remove the wet sodium sulphate, then the pure product was precipitated adding hexane to the solution and collected through Hirsch funnel filtration (261 mg; yield 81%).

^{1}H NMR (400 MHz, $CDCl_3$): 7.54–7.44 (m, 15H) ppm.

^{13}C NMR (100 Mhz, $CDCl_3$): 133.39 (C_3), 131.74 (C_1), 131.48 (C_4), 129.76 (C_2)ppm.

Elemental analysis: [calc. %] C: 34.31; H: 2.40 [found %] C: 34.16H: 2.18.

3.1.3. [AuI($SbPh_3$)] (3)

74 mg of commercially available [AuCl(SMe_2)] have been solubilized with 6 mL of dichloromethane in a 25 mL flask. Subsequently, 89 mg (1.0 eq.) of triphenylstibine were added and the resulting solution was stirred at room temperature. After 5 min, the dichloromethane was removed under reduced pressure and the solid residue was suspended in 5 mL of acetone. At this point, 100 mg (2.50 eq.) of KI were added to the suspension and the resulting mixture was stirred for 1 h. At the end of reaction time, the solvent was removed through a rotary evaporator and the crude product was solubilized in dichloromethane. The solution was washed in a separation funnel with water and brine, then the organic phase was dried with anhydrous sodium sulphate. The resulting suspension was filtered to remove the wet sodium sulphate, then the pure product was precipitated adding hexane to the solution and collected through Hirsch funnel filtration (121 mg; yield 71%).

^{1}H NMR (400 MHz, $CDCl_3$): 7.54–7.44 (m, 15H).

^{13}C NMR (100 MHz, $CDCl_3$): 133.41(C_3), 131.97 (C_1), 131.38 (C_4), 129.74(C_2) ppm.

Elemental analysis: [calc. %] C: 31.94; H: 2.23 [found %] C: 32.21H: 2.17.

3.2. XRD analysis

X-ray data collection was performed with a Bruker D8 Venture equipped with an IμS 3.0 Microfocus Incoatec Source and a Photon III Detector. Mo Kα radiation was used for the data collection performed at a temperature of 100 K, controlled using a CryoStream 700 (Oxford Cryosystems). For [Au($AsPh_3$)I] a total of 672 frames were collected. The total exposure time was 1.87 h. For [AuI($SbPh_3$)] a total of 546 frames were collected. The total exposure time was 0.39 h. The frames were integrated with the Bruker SAINT software package using a narrow-frame algorithm. Absorption correction was achieved through SADABS 2016/2 included in the Bruker Package of data treatment [56]. The structure was solved with the Shelxt Program and refined with SHELXL by full-matrix least-squares techniques with anisotropic displacement parameters for all non-hydrogen atoms [57].

3.3. LogP determination

LogP values were determined through a modification of the shake-flask method [58]. Water (50 mL, distilled after milli-Q purification) and n-octanol (50 mL) were shaken together for 72 h to allow saturation of both phases. About 1–3 mg of the [AuI(LPh_3)] complex were dissolved in a 15 mL Falcon tube in the octanol phase and then an equal volume of water was added. The mixture was hand shaken for ten minutes, and then centrifuged for five minutes at 6000 rpm to allow separation. Subsequently, 0.5 mL of each phase were moved in two different mineralization PE tubes together with 1 mL of metal-free concentrated nitric acid. The mixtures were heated overnight at 90 °C, then diluted with 4.5 mL of ultrapure water. Gold concentration in both phases was determined by ICP-OES. Reported logP is defined as log[complex]o/[complex]w. Final values were reported as the mean of three determinations.

3.4. IR experiments

5 mg of the [AuI(LPh_3)] complex and 1.1 eq of L-cysteine hydrochloride monohydrate were dissolved in 2 mL of DMSO in a 10 mL flask, and the reaction was stirred for 2 h at room temperature. After the solvent evaporation under reduced pressure, the solid residue was dissolved in liquid paraffin and analyzed in nujol.

3.5. NMR experiments

All NMR spectra were acquired on a JEOL 400YH spectrometer (resonating frequencies: 400, 160 and 100 MHz for ^{1}H, ^{31}P and ^{13}C,

respectively). All spectra were recorded at room temperature (25 ± 2 °C) in solvents with a deuteration degree of 99.8% and calibrated on solvent residual signals [59]. All deuterated solvents were purchased from Deutero.de (https://www.deutero.de/). ^{1}H, ^{31}P and ^{13}C characterisation spectra were recorded in $CDCl_3$. Conversely, a small amount of each compound has been solubilized in 0.5 mL of DMSO-d_6 to perform stability studies in DMSO solution.

For the interaction studies with cysteine, 3 mg of L-cysteine hydrochloride monohydrate and 1.1 equivalents of [AuI(LPh_3)] complex were dissolved in 0.5 mL of deuterated DMSO-d_6 in an NMR tube. The reaction was monitored through ^{31}P NMR and ^{13}C NMR at t_0 and after incubation at 37 °C for 24 h.

3.6. ESI-MS experiments

Dimethyl sulfoxide (DMSO) and 1,4-dithiothreitol (DTT) were purchased from Fluka. ESI-MS materials (water, methanol, and ammonium acetate) were purchased from Sigma-Aldrich. Lyophilized HSA, hCA I and SOD were purchased from Sigma-Aldrich and used without further purification or manipulation.

3.6.1. Interaction studies with cysteine and selenocysteine

Stock solutions in LC-MS grade DMSO were freshly prepared for cysteine (10^{-2} M), selenocystine (10^{-1} M), DTT (5×10^{-1} M) and [AuI(LPh_3)] complexes (10^{-2} M).

For cysteine experiments, suitable amounts of the previously prepared stock solutions were mixed in an Eppendorf tube in 1:1 metal: cysteine ratio and diluted with DMSO until a final concentration of cysteine 10^{-4} M. The solutions were kept at 37 °C for 2 h and then ESI-MS analysis was carried out. All samples were diluted to a final concentration of 5×10^{-6} M with a 20 mM ammonium acetate solution.

For selenocysteine experiments, suitable amounts of the previously prepared stock solutions were mixed in an Eppendorf tube in 2:1:10 metal:selenocystine:DTT ratio and diluted with DMSO until a final concentration of selenocysteine 10^{-4} M. The solutions were kept at 37 °C for 24 h and then ESI-MS analysis was carried out. All samples were diluted to a final concentration of 5×10^{-6} M with a 20 mM ammonium acetate solution.

3.6.2. Interaction studies with proteins

Stock solutions of HSA, hCA I and SOD 10^{-3} M were prepared, dissolving the proteins in LC-MS grade water. Stock solutions 10^{-2} M of the [AuI(LPh_3)] compounds were prepared by dissolving the samples in DMSO. Suitable amounts of the previously prepared stock solutions were mixed in an Eppendorf tube in 2:1 metal:protein ratio and diluted with a 20 mM ammonium acetate solution until a final concentration of protein 10^{-4} M. The solutions were kept at 37 °C for 4 h and then ESI-MS analysis was carried out. All samples were diluted to a final concentration of 5×10^{-7} M for hCA I and SOD with a 20 mM ammonium acetate solution, and to a final concentration of 10^{-6} M for HSA with a 20 mM ammonium acetate and 0.1% of formic acid.

3.6.3. ESI-MS acquisition

All the ESI mass spectra were recorded using a TripleTOF® 5600^{+} high-resolution mass spectrometer (Sciex, Framingham, MA, USA), equipped with a DuoSpray® interface operating with an ESI probe. The spectra were acquired through direct injection at 7 μL min^{-1} flow rate. The ESI source parameters are as follows:

Cysteine and selenocysteine: positive polarity; ion-spray voltage floating (ISFV) 5500 V; temperature (TEM) 25 °C; ion source gas 1 (GS1) 25 L min^{-1}; ion source gas 2 (GS2) 0 L min^{-1}; curtain gas (CUR) 20 L min^{-1}; collision energy (CE) 10 V; declustering potential (DP) 300 V; acquisition range 100–1000 *m/z*.

SOD: positive polarity; ion-spray voltage floating (ISFV) 5500 V; temperature (TEM) 25 °C; ion source gas 1 (GS1) 40 L min^{-1}; ion source gas 2 (GS2) 0 L min^{-1}; curtain gas (CUR) 15 L min^{-1}; declustering potential (DP) 200 V; collision energy (CE) 10 V; acquisition range 1500–3500 *m/z*.

hCA I: positive polarity; ion-spray voltage floating (ISFV) 5500 V; temperature (TEM) 25 °C; ion source gas 1 (GS1) 50 L min^{-1}; ion source gas 2 (GS2) 0 L min^{-1}; curtain gas (CUR) 20 L min^{-1}; declustering potential (DP) 50 V; collision energy (CE) 10 V; acquisition range 600–1400 *m/z*.

HSA: positive polarity; ion-spray voltage floating (ISVF) 5500 V; temperature (TEM) 37 °C; ion source gas 1 (GS1) 40 L min^{-1}; ion source gas 2 (GS2) 0 L min^{-1}; curtain gas (CUR) 30 L min^{-1}; declustering potential (DP) 200 V; collision energy (CE) 10 V; acquisition range 800–1600 *m/z*.

For acquisition, Analyst TF software 1.7.1 (Sciex) was used and deconvoluted spectra were obtained by using the Bio Tool Kit microapplication v.2.2 embedded in PeakView™ software v.2.2 (Sciex).

3.7. Biological experiments

3.7.1. Cell culture

A2780 human ovarian cancer cell line was purchased from Creative Bioarray (NY 11967, USA) (Lot N° CSC-C9491J), SKOV-3 human ovarian cancer cell line was gifted from Prof. Enrico Mini (University of Florence, Italy), and normal human skeletal myoblasts (HSkM) was purchased from Thermo Fisher Scientific Inc. (Lot N° 2007603). A2780 and SKOV-3 cell lines were grown in RPMI1640 medium supplemented with 10% FBS, 1% glutamine and 1% antibiotics at 37 °C and subcultured twice weekly. Split 1: 5 (3–6 × 10^4 cells per mL). Cryopreserved HSkM cells were directly plated in DMEM medium supplemented with 10% FBS, 1% glutamine and 1% antibiotics and used for cytotoxicity experiments only. All cell lines have been routinely tested for mycoplasma.

3.7.2. Cell viability assay

The inhibition of cell proliferation was evaluated through MTT (3-(4,5-dimethylthiazol-2-yl)-2,5-diphenyltetrazolium bromide) test. Briefly, 1 × 10^4 exponentially growing A2780 and SKOV-3 cells were seeded in 96 well-microplates for 24 h, then treated with gold compounds and cisplatin concentrations ranging from 0.003 to 100 μM and incubated for 72 h at 37 °C in a humidified incubator. Regarding the normal HSkM cells, 5 × 10^4 cells were seeded in 96 well-microplates. After 72 h of exposure, all cell lines were treated with 0.5 mg/mL MTT for 1 h at 37 °C. Following precipitation, blue formazan was dissolved in DMSO, and optical density was read at 595 nm in a microplate reader interfaced with Microplate Manager/PV version 4.0 software (BioRad Laboratories). From Absorbance measurements, half-maximal inhibitory concentration (IC_{50}) values of each compound were calculated by using GraphPad Prism Software 6.0 (Graphpad Holdings, LLC, USA). MTT test was performed in triplicate.

3.7.3. Thioredoxin reductase activity assay

The thioredoxin reductase (TrxR) activity was assessed by using a commercial colorimetric assay kit (Sigma Aldrich CS0170) based on the reduction of 5,5′-dithio-*bis*-(2-nitrobenzoic) acid (DTNB) with NADPH to 5-thio-2-nitrobenzoic acid (TNB) at 412 nm. Since several enzymes present in biological samples can reduce DTNB, the kit also contains an inhibitor solution of mammalian thioredoxin reductase. This inhibitor allows determining the reduction of DTNB due only to TrxR activity. A2780 cells were treated for 8 h with concentrations corresponding to their 72 h-exposure IC_{50}-doses and then lysed with RIPA buffer (50 mM Tris-HCl pH 7.0, 1% (*v*/v) NP-40, 150 mM NaCl, 2 mM ethylene glycol bis(2-aminoethyl ether)tetra-acetic acid, 100 mM NaF) supplemented with a protease inhibitor cocktail. The protein concentrations in the cell lysates were determined by Bradford protein assay kit (Bio-Rad Laboratories) according to the manufacturer's instructions and then 60 μg of proteins were used for the assay. Results were normalized to the cellular protein content. The experiments were performed in triplicate (three

independent biological replicates). The statistical analysis was carried out using one-way ANOVA test followed by Tukey's multiple comparisons test using GraphPad Prism software v 6.0. ANOVA-value $p < 0.05$ was considered statistically significant.

4. Conclusions

This paper describes the synthesis and the characterisation of a new panel of auranofin-inspired molecules, placing a strong emphasis on the ligands' modifications and their consequential impact on biological activity. Of particular note was the profound influence of ligand variation, including phosphine, arsine, and stibine ligands, on the stability in aqueous environment, lipophilicity and cytotoxicity of these analogues.

The reactivity against some reduced molecular models, such as cysteine and selenocysteine as a mimic for the thioredoxin reductase, has been investigated through NMR and IR spectroscopy. All the new compounds rapidly interact with the amino acids. Moreover, the reactivity has been evaluated also with some biologically relevant proteins (HSA, hCA I and SOD). In the case of compound **1**, HSA formed stable adducts with the reactive fragment $[Au(PPh_3)]^+$ while compounds **2** and **3** only showed protein metalation with a nude Au atom. This behaviour was perfectly in agreement with the decreasing bond strengths of Au with P, As and Sb. These interaction studies allowed us to gain insights into potential mechanisms of action and target engagement, shedding light on the specific interactions that underlie their cytotoxic effects.

Finally, the evaluation of the biological activity of this panel of molecules has been carried out on A2780S/R and SKOV-3 ovarian cancer cells, in comparison to the parent compound auranofin and cisplatin as reference. Compound **1** bearing the phosphine ligands emerged as the most potent, with IC_{50} values lower with respect to those of cisplatin. Interestingly, this compound also showed a very good selectivity for healthy cells. In addition, compound **1** showed an important effect on the TrxR inhibition in *in vitro* experiments, suggesting that its biological effect could be effectively exerted through the inhibition of this enzyme.

Although the results clearly showed that there are no synergistic effects related to the presence of different elements in the molecules, at the same time $[AuI(PPh_3)]$ emerged among the others as a potential anticancer molecule.

These findings collectively underscore the promising avenue for the development of more effective and selective gold-based anticancer agents, thereby addressing some of the limitations associated with conventional chemotherapy.

In conclusion, this research highlights not only the pivotal role of ligand variation in tailoring the biological activity of auranofin analogues but also underscores the exciting prospects for future drug development in the realm of cancer therapy. Nevertheless, further investigations, including rigorous *in vivo* studies, are imperative to harness the full therapeutic potential of these compounds and facilitate their translation into clinical applications.

CRediT authorship contribution statement

Ester Giorgi: Data curation, Investigation, Writing – original draft. **Michele Mannelli:** Investigation, Writing – original draft. **Tania Gamberi:** Data curation, Investigation, Writing – original draft. **Maria Durante:** Investigation. **Chiara Gabbiani:** Funding acquisition, Supervision. **Damiano Cirri:** Data curation, Supervision, Writing – original draft. **Alessandro Pratesi:** Conceptualization, Funding acquisition, Supervision, Writing – review & editing.

Declaration of Competing Interest

The authors declare the following financial interests/personal relationships which may be considered as potential competing interests:

Alessandro Pratesi reports financial support was provided by University of Pisa. Damiano Cirri reports financial support was provided by European Union. Alessandro Pratesi reports a relationship with University of Pisa that includes: employment and funding grants.

Data availability

Data will be made available on request.

Acknowledgements

AP gratefully acknowledges funding by the University of Pisa under the "PRA–Progetti di Ricerca di Ateneo" (Institutional Research Grants), project no. PRA_2022-2023_12 "New challenges of transition metal and lanthanide complexes in the perspective of green chemistry". DC acknowledge the support of the European Union by the Next Generation EU project ECS00000017 'Ecosistema dell'Innovazione' Tuscany Health Ecosystem (THE, PNRR, Spoke 4: Nanotechnologies for diagnosis and therapy). Professor Luigi Messori (Dept. of Chemistry "U. Schiff," University of Florence) is acknowledged for making available the TripleTOF® 5600^+ mass spectrometer. The Centre for Instrumentation Sharing (CISUP), University of Pisa, is also acknowledged for ESI-MS analysis.

Appendix A. Supplementary data

Electronic Supplementary Information (ESI) available: NMR spectra; in solution stability studies; ESI-MS spectra; XRD data and Uv-Vis experimental details. The CCDC deposition numbers for complexes **2** and **3** were 2296797 and 2296798, respectively. The data can be obtained free of charge via http://www.ccdc.cam.ac.uk, or from the Cambridge Crystallographic Data Centre, 12 Union Road, Cambridge CB21EZ, UK (Fax: (+44) 1223–336-033; *E*-mail: deposit@ccdc.cam.ac.uk). Supplementary data to this article can be found online at https://doi.org/10.1016/j.jinorgbio.2023.112452.

References

[1] E.J. Anthony, E.M. Bolitho, H.E. Bridgewater, O.W.L. Carter, J.M. Donnelly, C. Imberti, E.C. Lant, F. Lermyte, R.J. Needham, M. Palau, P.J. Sadler, H. Shi, F.-X. Wang, W.-Y. Zhang, Z. Zhang, Metallodrugs are unique: opportunities and challenges of discovery and development, Chem. Sci. 11 (2020) 12888–12917, https://doi.org/10.1039/D0SC04082G.

[2] S. Rottenberg, C. Disler, P. Perego, The rediscovery of platinum-based cancer therapy, Nat. Rev. Cancer 21 (2021) 37–50, https://doi.org/10.1038/s41568-020-00308-y.

[3] L. Galluzzi, I. Vitale, J. Michels, C. Brenner, G. Szabadkai, A. Harel-Bellan, M. Castedo, G. Kroemer, Systems biology of cisplatin resistance: past, present and future, Cell Death Dis. 5 (2014) e1257, https://doi.org/10.1038/cddis.2013.428.

[4] S. Ghosh, Cisplatin: the first metal based anticancer drug, Bioorg. Chem. 88 (2019), 102925, https://doi.org/10.1016/j.bioorg.2019.102925.

[5] F. Binacchi, C. Elia, D. Cirri, C. Van de Griend, X.-Q. Zhou, L. Messori, S. Bonnet, A. Pratesi, T. Biver, A biophysical study of the interactions of palladium(ii), platinum(ii) and gold(iii) complexes of aminopyridyl-2,2′-bipyridine ligands with RNAs and other nucleic acid structures, Dalton Trans. 52 (2023) 598–608, https://doi.org/10.1039/D2DT03483B.

[6] E. Barresi, I. Tolbatov, T. Marzo, E. Zappelli, A. Marrone, N. Re, A. Pratesi, C. Martini, S. Taliani, F. Da Settimo, D. La Mendola, Two mixed valence diruthenium(II,III) isomeric complexes show different anticancer properties, Dalton Trans. 50 (2021) 9643–9647, https://doi.org/10.1039/D1DT01492G.

[7] E. Barresi, I. Tolbatov, A. Pratesi, V. Notarstefano, E. Baglini, S. Daniele, S. Taliani, N. Re, E. Giorgini, C. Martini, F. Da Settimo, T. Marzo, D. La Mendola, A mixed-valence diruthenium(ii,iii) complex endowed with high stability: From experimental evidence to theoretical interpretation, Dalton Trans. 49 (2020) 14520–14527, https://doi.org/10.1039/d0dt02527e.

[8] A. Pratesi, D. Cirri, M.D. Đurović, S. Pillozzi, G. Petroni, Ž.D. Bugarčić, L. Messori, New gold carbene complexes as candidate anticancer agents, BioMetals. 29 (2016) 905–911, https://doi.org/10.1007/s10534-016-9962-0.

[9] E. Giorgi, F. Binacchi, C. Marotta, D. Cirri, C. Gabbiani, A. Pratesi, Highlights of new strategies to increase the efficacy of transition metal complexes for cancer treatments, Molecules. 28 (2023), https://doi.org/10.3390/molecules28010273.

[10] E. Boros, P.J. Dyson, G. Gasser, Classification of metal-based drugs according to their mechanisms of action, Chem. 6 (2020) 41–60, https://doi.org/10.1016/j.chempr.2019.10.013.

[11] Y. Lu, X. Ma, X. Chang, Z. Liang, L. Lv, M. Shan, Q. Lu, Z. Wen, R. Gust, W. Liu, Recent development of gold(I) and gold(III) complexes as therapeutic agents for

cancer diseases, Chem. Soc. Rev. 51 (2022) 5518–5556, https://doi.org/10.1039/D1CS00933H.
[12] G. Moreno-Alcántar, P. Picchetti, A. Casini, Gold complexes in anticancer therapy: from new design principles to particle-based delivery systems, Angew. Chem. 135 (2023), e202218000, https://doi.org/10.1002/ange.202218000.
[13] V. Fernández-Moreira, R.P. Herrera, M.C. Gimeno, Anticancer properties of gold complexes with biologically relevant ligands, Pure Appl. Chem. 91 (2019) 247–269, https://doi.org/10.1515/pac-2018-0901.
[14] T. Gamberi, G. Chiappetta, T. Fiaschi, A. Modesti, F. Sorbi, F. Magherini, Upgrade of an old drug: Auranofin in innovative cancer therapies to overcome drug resistance and to increase drug effectiveness, Med. Res. Rev. 42 (2022) 1111–1146, https://doi.org/10.1002/med.21872.
[15] M. Yamashita, Auranofin: past to present, and repurposing, Int. Immunopharmacol. 101 (2021), 108272, https://doi.org/10.1016/j.intimp.2021.108272.
[16] T. Marzo, L. Massai, A. Pratesi, M. Stefanini, D. Cirri, F. Magherini, M. Becatti, I. Landini, S. Nobili, E. Mini, O. Crociani, A. Arcangeli, S. Pillozzi, T. Gamberi, L. Messori, Replacement of the Thiosugar of Auranofin with iodide enhances the anticancer potency in a mouse model of ovarian cancer, ACS Med. Chem. Lett. 10 (2019) 656–660, https://doi.org/10.1021/acsmedchemlett.9b00007.
[17] I. Tolbatov, D. Cirri, L. Marchetti, A. Marrone, C. Coletti, N. Re, D. La Mendola, L. Messori, T. Marzo, C. Gabbiani, A. Pratesi, Mechanistic insights into the anticancer properties of the Auranofin analog au(PEt3)I: a theoretical and experimental study, Front. Chem. 8 (2020) 812, https://doi.org/10.3389/fchem.2020.00812.
[18] D. Cirri, F. Bartoli, A. Pratesi, E. Baglini, E. Barresi, T. Marzo, Strategies for the improvement of metal-based chemotherapeutic treatments, Biomedicines. 9 (2021) 504, https://doi.org/10.3390/biomedicines9050504.
[19] D. Cirri, A. Geri, L. Massai, M. Mannelli, T. Gamberi, F. Magherini, M. Becatti, C. Gabbiani, A. Pratesi, L. Messori, Chemical modification of Auranofin yields a new family of anticancer drug candidates: the gold(I) phosphite analogues, Molecules. 28 (2023) 1050, https://doi.org/10.3390/molecules28031050.
[20] D. Cirri, L. Massai, C. Giacomelli, M.L. Trincavelli, A. Guerri, C. Gabbiani, L. Messori, A. Pratesi, Synthesis, chemical characterization, and biological evaluation of a novel auranofin derivative as an anticancer agent, Dalton Trans. 51 (2022) 13527–13539, https://doi.org/10.1039/D2DT00836J.
[21] T. Marzo, D. Cirri, C. Gabbiani, T. Gamberi, F. Magherini, A. Pratesi, A. Guerri, T. Biver, F. Binacchi, M. Stefanini, A. Arcangeli, L. Messori, Auranofin, et $_3$ PAuCl, and et $_3$ PAuI are highly cytotoxic on colorectal cancer cells: a chemical and biological study, ACS Med. Chem. Lett. 8 (2017) 997–1001, https://doi.org/10.1021/acsmedchemlett.7b00162.
[22] D. Cirri, M.G. Fabbrini, L. Massai, S. Pillozzi, A. Guerri, A. Menconi, L. Messori, T. Marzo, A. Pratesi, Structural and solution chemistry, antiproliferative effects, and serum albumin binding of three pseudohalide derivatives of auranofin, BioMetals 32 (2019) 939–948, https://doi.org/10.1007/s10534-019-00224-1.
[23] I. Landini, L. Massai, D. Cirri, T. Gamberi, P. Paoli, L. Messori, E. Mini, S. Nobili, Structure-activity relationships in a series of auranofin analogues showing remarkable antiproliferative properties, J. Inorg. Biochem. 208 (2020), 111079, https://doi.org/10.1016/j.jinorgbio.2020.111079.
[24] Z. Yin, Z. Deng, W. Zhao, Z. Cao, Searching synergistic dose combinations for anticancer drugs, Front. Pharmacol. 9 (2018) 535, https://doi.org/10.3389/fphar.2018.00535.
[25] A. Emadi, S.D. Gore, Arsenic trioxide — an old drug rediscovered, Blood Rev. 24 (2010) 191–199, https://doi.org/10.1016/j.blre.2010.04.001.
[26] P. Sharma, D. Perez, A. Cabrera, N. Rosas, J.L. Arias, Perspectives of antimony compounds in oncology, Acta Pharmacol. Sin. 29 (2008) 881–890, https://doi.org/10.1111/j.1745-7254.2008.00818.x.
[27] P. Baiocco, G. Colotti, S. Franceschini, A. Ilari, Molecular basis of antimony treatment in Leishmaniasis, J. Med. Chem. 52 (2009) 2603–2612, https://doi.org/10.1021/jm900185q.
[28] G. Colotti, A. Ilari, Antimony-based therapy of Leishmaniases, molecular and cellular rationale, in: R.H. Kretsinger, V.N. Uversky, E.A. Permyakov (Eds.), Encycl. Met, Springer, New York, New York, NY, 2013, pp. 78–86, https://doi.org/10.1007/978-1-4614-1533-6_545.
[29] S. Ahrland, K. Dreisch, B. Norén, Å. Oskarsson, A. Kankaanperä, Crystal structures of Iodo(triphenylphosphine)gold(I) and Bis[iodo(trimethylphosphine)gold(I)], Acta Chem. Scand. 41a (1987) 173–177, https://doi.org/10.3891/acta.chem.scand.41a-0173.
[30] P.F. Barron, L.M. Engelhardt, P.C. Healy, J. Oddy, A.H. White, Lewis-base adducts of group I metal(I) compounds. XXVI. Solid-state cross-polarization magic-angle-spinning 31P N.M.R. and structural studies on 1:1 adducts of triphenylphosphine with gold(I) salts, Aust. J. Chem. 40 (1987) 1545–1555, https://doi.org/10.1071/ch9871545.
[31] S.P.C. Dunstan, P.C. Healy, A.N. Sobolev, E.R.T. Tiekink, A.H. White, M. L. Williams, Isomorphism in the structural chemistry of two-coordinate adducts of diphenyl(2-formylphenyl)phosphine and triphenylphosphine with gold(I) halides, J. Mol. Struct. 1072 (2014) 253–259, https://doi.org/10.1016/j.molstruc.2014.05.020.
[32] D. Cirri, M.G. Fabbrini, A. Pratesi, L. Ciofi, L. Massai, T. Marzo, L. Messori, The leading established metal-based drugs: a revisitation of their relevant physico-chemical data, BioMetals. 32 (2019) 813–817, https://doi.org/10.1007/s10534-019-00210-7.
[33] M.P. Rigobello, G. Scutari, A. Folda, A. Bindoli, Mitochondrial thioredoxin reductase inhibition by gold(I) compounds and concurrent stimulation of permeability transition and release of cytochrome c, Biochem. Pharmacol. 67 (2004) 689–696, https://doi.org/10.1016/j.bcp.2003.09.038.
[34] V. Scalcon, A. Bindoli, M.P. Rigobello, Significance of the mitochondrial thioredoxin reductase in cancer cells: an update on role, targets and inhibitors, Free Radic. Biol. Med. 127 (2018) 62–79, https://doi.org/10.1016/j.freeradbiomed.2018.03.043.
[35] S. Urig, K. Becker, On the potential of thioredoxin reductase inhibitors for cancer therapy, Semin. Cancer Biol. 16 (2006) 452–465, https://doi.org/10.1016/j.semcancer.2006.09.004.
[36] K.P. Bhabak, B.J. Bhuyan, G. Mugesh, Bioinorganic and Medicinal Chemistry: Aspects of Gold(I)-Protein Complexes, 2011.
[37] L. Skos, C. Schmidt, S. Thomas, M. Park, R. Bonsignore, G. Del Favero, T. Mohr, A. Bileck, C. Gerner, A. Casini, S.M. Meier-Menches, Selective arylation of selenocysteine of thioredoxin reductase 1 by an organogold compound: expanding the tool-box of metal-templated reactions in cancer cells, Chemistry (2023), https://doi.org/10.26434/chemrxiv-2023-plbdr.
[38] C. Zoppi, L. Messori, A. Pratesi, ESI MS studies highlight the selective interaction of Auranofin with protein free thiols, Dalton Trans. 49 (2020) 5906–5913, https://doi.org/10.1039/D0DT00283F.
[39] L. Kou, S. Wei, P. Kou, Current progress and perspectives on using gold compounds for the modulation of tumor cell metabolism, Front. Chem. 9 (2021), 733463, https://doi.org/10.3389/fchem.2021.733463.
[40] F.H. Abdalbari, C.M. Telleria, The gold complex auranofin: new perspectives for cancer therapy, Discov. Oncol. 12 (2021) 42, https://doi.org/10.1007/s12672-021-00439-0.
[41] A. Balfourier, J. Kolosnjaj-Tabi, N. Luciani, F. Carn, F. Gazeau, Gold-based therapy: from past to present, Proc. Natl. Acad. Sci. 117 (2020) 22639–22648, https://doi.org/10.1073/pnas.2007285117.
[42] A. Pratesi, C. Gabbiani, E. Michelucci, M. Ginanneschi, A.M. Papini, R. Rubbiani, I. Ott, L. Messori, Insights on the mechanism of thioredoxin reductase inhibition by gold N-heterocyclic carbene compounds using the synthetic linear Selenocysteine containing C-terminal peptide hTrxR(488-499): an ESI-MS investigation, J. Inorg. Biochem. 136 (2014) 161–169, https://doi.org/10.1016/j.jinorgbio.2014.01.009.
[43] I. Tolbatov, D. Cirri, L. Marchetti, A. Marrone, C. Coletti, N. Re, D. La Mendola, L. Messori, T. Marzo, C. Gabbiani, A. Pratesi, Mechanistic insights into the anticancer properties of the Auranofin analog Au(PEt3)I: a theoretical and experimental study, Front. Chem. 8 (2020) 812, https://doi.org/10.3389/fchem.2020.00812.
[44] L. Chiaverini, A. Pratesi, D. Cirri, A. Nardinocchi, I. Tolbatov, A. Marrone, M. Di Luca, T. Marzo, D. La Mendola, Anti-staphylococcal activity of the Auranofin analogue bearing acetylcysteine in place of the Thiosugar: an experimental and theoretical investigation, Molecules. 27 (2022) 2578, https://doi.org/10.3390/molecules27082578.
[45] L. Zhong, E.S.J. Arnér, A. Holmgren, Structure and mechanism of mammalian thioredoxin reductase: the active site is a redox-active selenolthiol/selenenylsulfide formed from the conserved cysteine-selenocysteine sequence, Proc. Natl. Acad. Sci. 97 (2000) 5854–5859, https://doi.org/10.1073/pnas.100114897.
[46] K. Fritz-Wolf, S. Urig, K. Becker, The structure of human thioredoxin reductase 1 provides insights into C-terminal rearrangements during catalysis, J. Mol. Biol. 370 (2007) 116–127, https://doi.org/10.1016/j.jmb.2007.04.044.
[47] E. Delgado, E. Hernandez, Gold(I) complexes with thiolate and triphenylphosphine ligands, Polyhedron. 11 (1992) 3135–3138, https://doi.org/10.1016/S0277-5387(00)83654-2.
[48] J.C. Foster, C.R. Powell, S.C. Radzinski, J.B. Matson, S-Aroylthiooximes: a facile route to hydrogen sulfide releasing compounds with structure-dependent release kinetics, Org. Lett. 16 (2014) 1558–1561, https://doi.org/10.1021/ol500385a.
[49] C. Zhang, L. Gao, Q. Yuan, L. Zhao, W. Niu, P. Cai, J. Li, X. Han, Z. He, F. Gao, Y. Wang, H. Jiang, Z. Chai, X. Gao, Is GSH chelated Pt molecule inactive in anti-cancer treatment? A case study of Pt $_6$ GS $_4$, Small 16 (2020) 2002044, https://doi.org/10.1002/smll.202002044.
[50] L. Massai, C. Zoppi, D. Cirri, A. Pratesi, L. Messori, Reactions of medicinal gold(III) compounds with proteins and peptides explored by electrospray ionization mass spectrometry and complementary biophysical methods, Front. Chem. 8 (2020), 581648, https://doi.org/10.3389/fchem.2020.581648.
[51] A. Pratesi, D. Cirri, D. Fregona, G. Ferraro, A. Giorgio, A. Merlino, L. Messori, Structural characterization of a gold/serum albumin complex, Inorg. Chem. 58 (2019) 10616–10619, https://doi.org/10.1021/acs.inorgchem.9b01900.
[52] A. Casini, M.A. Cinellu, G. Minghetti, C. Gabbiani, M. Coronnello, E. Mini, L. Messori, Structural and solution chemistry, antiproliferative effects, and DNA and protein binding properties of a series of dinuclear gold(III) compounds with bipyridyl ligands, J. Med. Chem. 49 (2006) 5524–5531, https://doi.org/10.1021/jm060436a.
[53] T. Gamberi, A. Pratesi, L. Messori, L. Massai, Proteomics as a tool to disclose the cellular and molecular mechanisms of selected anticancer gold compounds, Coord. Chem. Rev. 438 (2021), 213905, https://doi.org/10.1016/J.CCR.2021.213905.
[54] X. Zhang, K. Selvaraju, A.A. Saei, P. D'Arcy, R.A. Zubarev, E.S. Arnér, S. Linder, Repurposing of auranofin: Thioredoxin reductase remains a primary target of the drug, Biochimie 162 (2019) 46–54, https://doi.org/10.1016/j.biochi.2019.03.015.
[55] A. Bindoli, M.P. Rigobello, G. Scutari, C. Gabbiani, A. Casini, L. Messori, Thioredoxin reductase: a target for gold compounds acting as potential anticancer drugs, Coord. Chem. Rev. 253 (2009) 1692–1707, https://doi.org/10.1016/J.CCR.2009.02.026.
[56] L. Krause, R. Herbst-Irmer, G.M. Sheldrick, D. Stalke, Comparison of silver and molybdenum microfocus X-ray sources for single-crystal structure determination, J. Appl. Crystallogr. 48 (2015) 3–10, https://doi.org/10.1107/S1600576714022985.

[57] G.M. Sheldrick, Crystal structure refinement with SHELXL, Acta Crystallogr. Sect. C Struct. Chem. 71 (2015) 3–8, https://doi.org/10.1107/S2053229614024218.
[58] D. Cirri, S. Pillozzi, C. Gabbiani, J. Tricomi, G. Bartoli, M. Stefanini, E. Michelucci, A. Arcangeli, L. Messori, T. Marzo, PtI $_2$ (DACH), the iodido analogue of oxaliplatin as a candidate for colorectal cancer treatment: chemical and biological features, Dalton Trans. 46 (2017) 3311–3317, https://doi.org/10.1039/C6DT03867K.
[59] G.R. Fulmer, A.J.M. Miller, N.H. Sherden, H.E. Gottlieb, A. Nudelman, B.M. Stoltz, J.E. Bercaw, K.I. Goldberg, NMR chemical shifts of trace impurities: common laboratory solvents, organics, and gases in deuterated solvents relevant to the organometallic chemist, Organometallics. 29 (2010) 2176–2179, https://doi.org/10.1021/om100106e.